Noninvasive Quantification of Retinal Microglia Using Widefield Autofluorescence Imaging

Despina Kokona, Nadia Schneider, Helena Giannakaki-Zimmermann, Joel Jovanovic, Andreas Ebneter, and Martin Zinkernagel

Department of Ophthalmology and Department of Clinical Research, Inselspital, Bern University Hospital, and University of Bern, Switzerland

Correspondence: Martin Zinkernagel, University Hospital Bern, 3010 Bern, Switzerland; m.zinkernagel@gmail.com.

Submitted: October 13, 2016
Accepted: March 15, 2017

Citation: Kokona D, Schneider N, Giannakaki-Zimmermann H, Jovanovic J, Ebneter A, Zinkernagel M. Noninvasive quantification of retinal microglia using widefield autofluorescence imaging. *Invest Ophthalmol Vis Sci*. 2017;58:2160–2165. DOI:10.1167/iovs.16-20916

Purpose. To validate widefield autofluorescence (AF) in vivo imaging of the retina in mice expressing green fluorescent protein (gfp) in microglia, and to monitor retinal microglia reconstitution in vivo after lethal irradiation and bone marrow transplantation.

Methods. Transgenic *Cx3cr1*$^{gfp/gfp}$ and wildtype Balb/c mice were used in this study. A confocal scanning laser ophthalmoscope was used for AF imaging with a 55° and a widefield 102° lens. Intrasession reproducibility was assessed for each lens. To investigate reconstitution in vivo, bone marrow from *Cx3cr1*$^{gfp/gfp}$ mice was used to rescue lethally irradiated wildtype mice. Data were compared to confocal microscopy of retinal flat mounts.

Results. Both the 55° and the 102° lens produced high resolution images of retinal microglia with similar microglia density. However, compared to the 55° lens, the widefield 102° lens captured approximately 3.6 times more microglia cells (1515 ± 123 cells versus 445 ± 76 cells [mean ± SD], for 102° and 55°, respectively, $P < 0.001$). No statistical difference in the number of gfp positive cells within corresponding areas was observed within the same imaging session. Imaging of microglia reconstitution showed a similar time course compared to flat mount preparations with an excellent correlation between microglia cell numbers in AF and gfp-stained flat mounts ($R = 0.92$, $P < 0.0001$).

Conclusions. Widefield AF imaging of mice with gfp expressing microglia can be used to quantify retinal microglia. In vivo microglia counts corresponded very well with ex vivo counts on retinal flat mounts. As such, AF imaging can largely replace ex vivo quantification.

Keywords: fundus autofluorescence, ophthalmic imaging, microglia, validation study

Microglia cells are found throughout the central nervous system. They are the major inflammatory cell type in the brain, and respond to pathogens and injury. When they become activated, they rapidly change morphology, proliferate, and migrate to the site of injury, where they remove pathogens, as well as damaged cells by phagocytosis. The retina as part of the central nervous system acts as a window to the brain. As such, imaging modalities allowing monitoring and quantifying inflammation in the retina reveal information, which might be extrapolated to central nervous system inflammation or age-related changes. There is growing evidence that systemic inflammatory stimuli, such as infection, can trigger activation of microglia by systemic release of proinflammatory mediators, such as cytokines.[1] This activation in turn may lead to exacerbation of neurologic diseases, such as Alzheimer's disease, but also retinal pathology like retinitis pigmentosa.[2,3] Thus, imaging of retinal microglia might serve as a tool to study the role of systemic microglia activation in neurodegenerative diseases.

In the retina, microglia reside as well-organized networks in the ganglion cell layer, the inner plexiform layer, and the outer plexiform layer.[4] Relatively little is known about microglia homeostasis in the retina, but depletion studies have shown that microglial cells are necessary for synaptic transmission.[5] Furthermore, microglia have been associated with various retinal diseases ranging from inherited photoreceptor degeneration, light-induced retinal degeneration, to glaucoma.[6–9] Increased numbers of activated microglia cells have been observed in retinal dystrophy models in rodents.[6,10,11] Given the importance of microglial cells in various retinal disorders and the recent revelations on the regeneration of microglia from within intrinsic pools,[12] in vivo imaging quantifying microglia might help the understanding of the role and the dynamics of these cells in retinal disease.

Facilitated by advancements in retinal imaging technology allowing visualization of ever larger areas of the retina, in vivo imaging of transgenic mice, where the *Cx3cr1* gene has been replaced by the green fluorescent protein (gfp) DNA sequence (*Cx3cr1*$^{gfp/gfp}$), might potentially replace flat mounts as the gold standard for quantification of retinal microglia. This would on one hand help reduce animal numbers required for experimental studies and, on the other hand, permit efficient longitudinal assessment of microglia density in the retina. However, as far as we are aware, there are no studies correlating widefield in vivo microglia imaging with flat mount data.[13] In order to fill this gap, we compared autofluorescence (AF) imaging of *Cx3cr1*$^{gfp/gfp}$ mice using different lenses to retinal flat mounts stained for gfp, and used this imaging method in wildtype mice to monitor retinal microglia reconstitution after lethal irradiation and rescue with bone marrow transplants from *Cx3cr1*$^{gfp/gfp}$ mice.

Materials and Methods

Animals

The present study was approved by the local Animal Ethics Committee (Veterinärdienst des Kantons Bern: BE 38/13) and conformed to the ARVO Statement for the Use of Animals in Ophthalmic and Vision Research. Fourteen male and female Balb/c AnNCrl mice (5–6 weeks of age, Charles River Laboratories, Sulzfeld, Germany) and 10 Balb/c-*Cx3cr1*$^{gfp/gfp}$ mice were used for this study.[14] Balb/c-*Cx3cr1*$^{gfp/gfp}$ mice were kindly provided by Steffen Jung (Weizmann Institute of Science, Rehovot, Israel).

Animals were housed in individually ventilated cages under temperature and humidity-controlled conditions with a 12-hour light/12-hour dark cycle. Anesthesia, necessary for imaging, was achieved by intraperitoneal (ip) injection of medetomidine (1 mg/kg, Dormitor 1 mg/mL, Provet AG, Lyssach, Switzerland) and ketamine (80 mg/kg, Ketalar 50 mg/mL, Parke-Davis, Zurich, Switzerland). At the end of the intervention, atipamezole (2.3 mg/kg Antisedan 5 mg/mL, Provet AG) was used to antagonize medetomidine. At the end of the experimental procedures, mice were euthanized with carbon dioxide (CO_2) inhalation. For each animal, one eye was kept for retinal flat mounts and the other eye was processed for paraffin embedding.

Generation of Bone Marrow Chimeras

Fourteen recipient Balb/c AnNCrl mice were lethally irradiated with two doses 14 hours apart, resulting in 6-Gy γ-ray full body irradiation. Four donor *Cx3cr1*$^{gfp/gfp}$ Balb/c mice were euthanized, and bone marrow cells were isolated. Recipient mice received a single intravenous injection of 2×10^6 bone marrow cells after 2 to 3 hours of the second dose of irradiation. Water supplemented with antibiotics (0.8 mg/mL sulfamethoxazole and 0.16 mg/mL trimethoprim) was provided in the drinking water to chimera mice for 2 weeks after the transplantation.

AF Imaging

Green fluorescent protein-positive microglia/macrophages in the retina of *Cx3cr1*$^{gfp/gfp}$ Balb/c mice were imaged with AF at two time points (T1 and T2) 14 ± 7 days apart. Anesthetized mice were placed on a custom-made platform positioned on the forehead rest of the Heidelberg Spectralis device (Heidelberg Engineering GmbH, Heidelberg, Germany). To keep the cornea hydrated during the imaging session, hydroxypropylmethylcellulose (Methocel 2%; OmniVision, Neuhausen, Switzerland) was applied regularly to both eyes. Before AF imaging, the big retinal vessels of the eye fundus were brought into focus using the infrared mode of the Spectralis to ensure that the same retinal layers will be imaged in all mice. Furthermore, the center of the optic nerve was centered in the image. AF images were acquired at a high resolution (approximately 6 μm/pixel)[15] of 1536×1636 pixels using the widefield 102° or 55° lens mounted on a Heidelberg Spectralis device. The focusing power of the Spectralis device was set to 25.8 ± 5.3 diopters (mean ± SD). For image acquisition in the same session, the image was aligned manually with the previously recorded image as the true-track mode was not available. An additional contact lens did not improve image quality and was not used.

Quantification of Microglia Cells

Green fluorescent protein-positive cells were quantified using the free ImageJ 1.44 software.[16] Briefly, the background was subtracted from the 8-bit images, the threshold was adjusted, and a binary mask was created. Overlays of the original and the binary image were created to ensure that only gfp-positive cells were quantified on the binary image and not background as well. Cells were quantified using the "analyze particles" function (Supplementary Fig. S1C). Only particles of an area greater than 30 μm^2 were included in the quantification. Autofluorescent cells were counted in the area visualized with the 55° or 102° lens. For comparison, the retinal area imaged with the 55° lens was compared to the corresponding retinal area in the 102° image. The same was done when comparing the 102° images with flat mount histology. Selection of corresponding retinal areas was based on vessel architecture or on identification of cell motifs when comparing the 55° with the 102° widefield lens (Supplementary Figs. S1A, S1B).

Immunohistochemical Studies—Retinal Flat Mounts

At selected time points (T2 for the *Cx3cr1*$^{gfp/gfp}$ and 5, 8, or 10 weeks after bone marrow transplantation for the chimera mice), mice were euthanized, their eyes were removed and fixed in 4% paraformaldehyde (PFA) solution (pH 7.4) for 10 minutes. The cornea and the lens were removed, and the eyecup, including the retina, choroid, and sclera, was incubated for 50 more minutes in 4% PFA. Retinas were detached from the choroid, washed in 0.1% Triton phosphate-buffered saline (PBS-T), and incubated in 5% normal goat serum in PBS-T for 2 hours at room temperature. Isolectin GS-IB4 from Griffonia simplicifolia, Alexa Fluor 647 conjugate (1:100 in 5% normal goat serum in 0.1% PBS-T, Thermo Fisher Scientific, Waltham, MA, USA) and a chicken polyclonal antibody against gfp (1:100, ab13970, Abcam, Cambridge, UK) were used for the labelling of blood vessels and gfp-positive microglia/macrophages, respectively. A rabbit polyclonal antibody against ionized calcium-binding adapter molecule 1 (Iba-1, 1:500, 016-20001, Wako Chemicals, Richmond, VA, USA) was used for the detection of microglia cells. Retinas were incubated in the antibody pool for 48 hours at 4°C. A secondary goat anti-rabbit IgG (H+L), Alexa Fluor 594 conjugate (1:1000, A27016, Thermo Fisher Scientific) and a preabsorbed goat polyclonal to chicken IgY H&L (FITCH; 1:1000, ab7114, Abcam) were used for the visualization of Iba-1 and gfp immunoreactive cells, respectively. Radial cuts were made on the retinas, and finally tissues were flat mounted on a slide with the ganglion cell layer facing up. Retinal flat mounts were cover-slipped with VECTASHIELD Antifade Mounting Medium (Vector Laboratories, Burlingame, CA, USA) and observed under the microscope.

To obtain retinal slices, eyes from euthanized mice were fixed in 4% PFA (pH 7.4) overnight and then processed for routine paraffin embedding. Slices of 5 μm containing the optic nerve head were cut with a microtome (Leica, Biosystems, Muttenz, Switzerland) and collected on glass slides (Menzel SuperFrost, Thermo Fisher Scientific). A rabbit polyclonal antibody against Iba-1 (1:5000, 016-20001, Wako Chemicals) and a chicken polyclonal antibody against gfp (1:100, ab13970, Abcam) were used for the staining of microglia/macrophages. The secondary antibodies goat anti-rabbit IgG (H+L), Alexa Fluor 594 conjugate (1:1000, A27016, Thermo Fisher Scientific) and chicken IgY H&L (FITCH; 1:1000, ab7114, Abcam) were used for the visualization of Iba-1 and gfp immunoreactivity, respectively. Slides were mounted in mounting medium with DAPI (Vector Laboratories), cover slipped, and observed in the microscope.

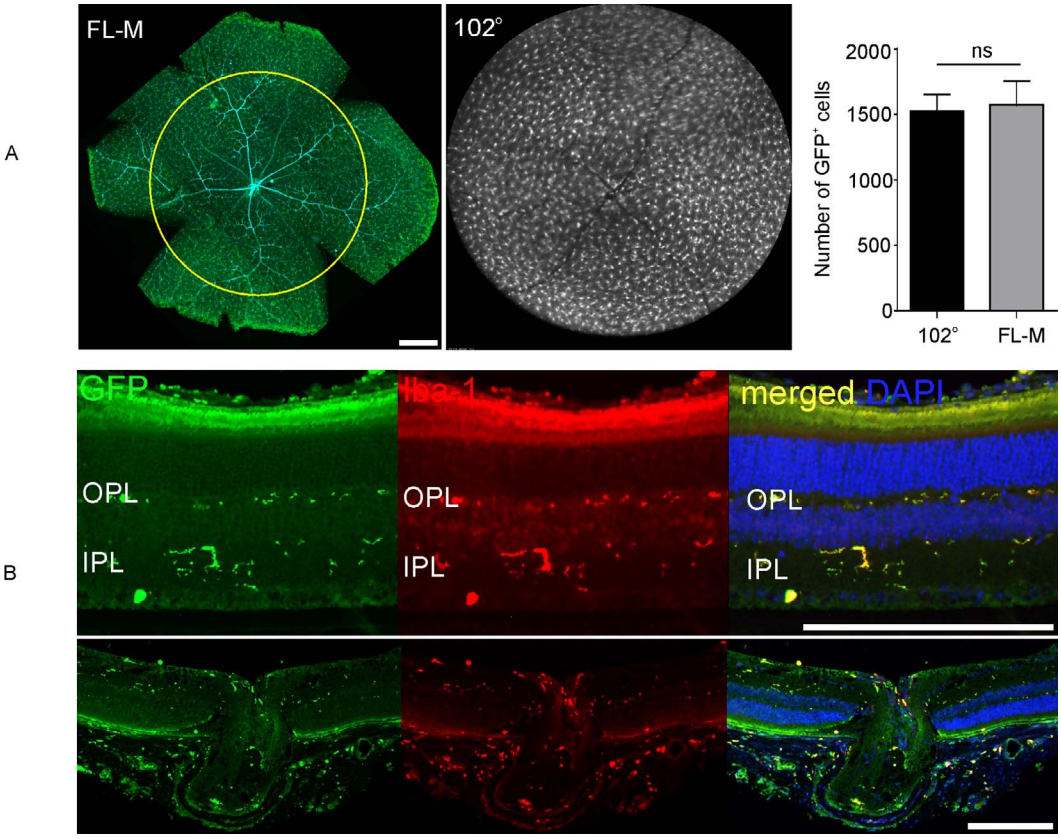

Figure 1. Identification of retinal microglia with different imaging modalities. (**A**) Identification of gfp-positive cells using retinal flat mount (*left*) and widefield imaging (*right*). The widefield 102° lens covers approximately 50% of the flat mount images (*yellow circle* on flat mount image). Quantification of the number of gfp-positive cells in 102° images and flat mount images of corresponding areas (102° image and area inside the *yellow circle* on the flat mount image, $n = 5$, $P > 0.05$, paired *t*-test). (**B**) In Balb/c AnNCrl-*Cx3cr1*$^{gfp/gfp}$ mice, all gfp-positive cells were co-localized with the microglia marker Iba-1 ($n = 5$). The majority of these cells were localized in the outer and inner plexiform layer. FL-M, flat mount, *scale bars*: 500 μm (**A**), 200 μm (**B**). IPL, inner plexiform layer; OPL, outer plexiform layer.

Microscopy

A Zeiss LSM 710 fluorescence confocal microscope (Carl Zeiss, Oberkochen, Germany) was used for imaging of retinal flat mounts. Z-stacks of 47.8 ± 9.2 μm of tissue (mean ± SD) with a 1-μm interval were obtained and finalized with the Imaris 7.1 software (Bitplane AG, Zurich, Switzerland). The final figures were prepared in CorelDraw (Corel Draw X7, Corel Corporation, Ottawa, Canada).

Statistics

GraphPad Prism 5.0 software (GraphPad Software, Inc., San Diego, CA, USA) was used for the statistical analysis. Before parametric statistics, D'Agostino-Pearson or Kolmogorov-Smirnov normality tests were performed. Statistically significant differences of gfp-positive cell numbers between different lenses were determined, and paired *t*-tests were used to compare different lenses or to compare AF data with flat mount data. Longitudinal data were analyzed using ordinary 1-way ANOVA followed by Tukey's post hoc analysis. *P* values < 0.05 were considered statistically significant. Pearson correlation was used to compare data between AF and flat mount histology in the bone marrow chimera mice. To test for reproducibility, intraclass correlation (ICC) type 2 was calculated for the data derived during the same imaging session (T1 and T2) with the same lens (55° or 102°). All gfp-positive cell quantification results are presented as mean ± SD on the graphs and throughout the article.

Results

Quantification of Microglia Cells Using Widefield AF Imaging

Areas obtained with the 102° lens corresponded to 51.8 ± 5.8% (mean ± SD) of the flat mounted retina (Fig. 1A, yellow circle on FL-M image). Quantification of gfp-expressing cells in 102° images and corresponding areas of retinal flat mounts did not reveal any statistically significant difference in the number of these cells between the two modalities (Fig. 1A, bar graph, $P > 0.05$). All gfp-positive cells were co-localized with the microglia marker Iba-1 and were found mainly in the inner and outer plexiform layers of the Balb/c-*Cx3cr1*$^{gfp/gfp}$ mouse retina (Fig. 1B).

Comparison of Two Different Widefield Lenses for the Quantification of Retinal Microglia Using AF

To test for reproducibility, AF images of the mouse fundus were obtained with a 55° and a 102° lens at two different time points (T1 and T2 in Fig. 2A). The 55° lens could cover 35.6 ± 3.8% (mean ± SD) of the fundus area imaged with the 102° lens (Fig. 2A, yellow circle on 102° images). The ICC was 0.65 for the 55° lens and 0.55 for the 102° lens. No statistically significant difference in the number of gfp-positive cells was observed between different time points (Fig. 2B, top graph) or between the two lenses when comparing corresponding areas (Fig. 2B, bottom left graph). However, as expected, approximately 3.6

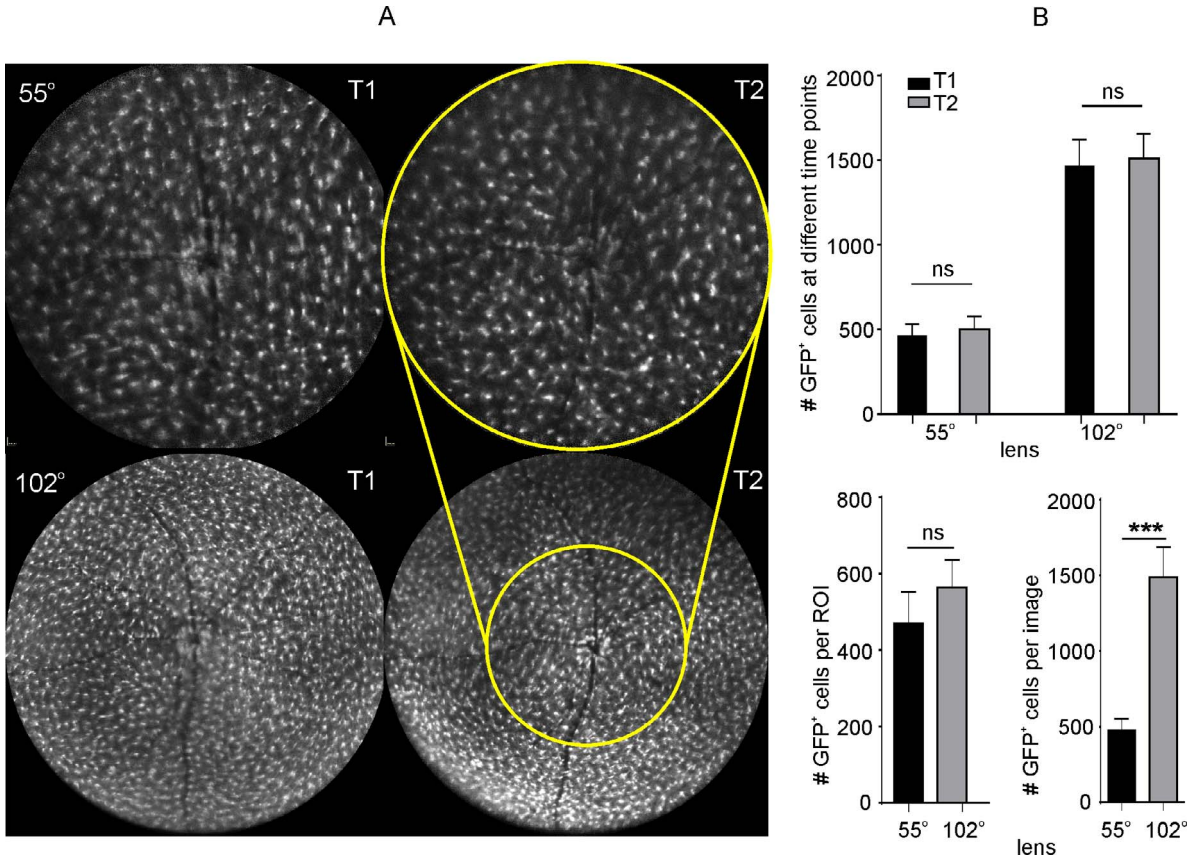

Figure 2. Quantification of retinal microglia with AF. (**A**) Representative AF images obtained with a 55° (*top panels*) and a 102° lens (*bottom panels*) at two different time points (T1 and T2). The pictures derived from the 55° lens represent almost 36% of the 102° lens images (*yellow circle* on 102° lens image). (**B**) Quantification of gfp-positive cells at two different time points (T1 and T2) with the 55° and the 102° widefield lens (*top graph*, $n = 10$ per time point, $P > 0.05$, paired *t*-test). *Bottom left graph*; Quantification of gfp-positive cells within corresponding regions of interest (ROI; *yellow circles*) within the 55° and the 102° images ($n = 10$ per imaging group, $P > 0.05$, paired *t*-test). *Bottom right graph*; the total number of gfp-positive cells imaged with the 55° and the widefield 102° lens ($n = 10$ $^{***}P < 0.001$, paired *t*-test). T1, time point 1; T2, time point 2; ROI, region of interest; ns, not significant.

times more gfp-positive cells were seen with the 102° lens compared to the 55° lens (Fig. 2B, bottom right graph).

Replenishment Dynamics of Retinal Microglia After Lethal Irradiation and Bone Marrow Reconstitution Imaged With Widefield AF and Correlation With Flat Mount Data

Bone marrow chimera mice were monitored with AF at 5, 8, and 10 weeks after bone marrow transplantation. Longitudinal imaging revealed gfp-positive cells around the optic nerve as early as 3 weeks posttransplantation (data not shown). The number of gfp-positive cells gradually increased (Figs. 3A, 3B, left graph, blue line) and reached approximately 37.2% of the number observed in the normal retina by week 10 (1515 ± 49 cells in the normal retinas versus 564 ± 73 cells in chimera retinas 10 weeks after bone marrow transplantation, $P < 0.001$). Likewise, there was a gradual replenishment of retinal microglia seen in flat mounts stained for gfp (Fig. 3B, left graph, red line), with gfp-positive cell numbers at week 10 reaching approximately 36% of the levels found in untreated mice (1562 ± 87 cells in the untreated retinas versus 556 ± 80 cells in chimera retinas 10 weeks after bone marrow transplantation, $P < 0.001$). All gfp-positive cells were also Iba-1 positive (data not shown). The same profile of gfp-positive cells infiltration was observed in retinal flat mounts and AF images (Fig. 3A). There was a good correlation ($r = 0.92$, $P < 0.0001$) when comparing replenishment dynamics observed in AF and data from retinal flat mounts stained for gfp (Fig. 3B, right graph).

Microglia Cells Are Equally Distributed Between the Central and the Peripheral Retina

Green fluorescent protein-positive cells were separately quantified in the central (Fig. 4, left panel, center, area obtained with the 55° lens) and peripheral retina (Fig. 4, left panel, periphery, area obtained with the 102° lens minus area obtained with the 55° lens). No statistically significant differences were observed in gfp-positive cell density in the central and peripheral retina (Fig. 4, right graph, $P > 0.05$, paired *t*-test).

Discussion

Here, we confirm that widefield AF imaging of gfp-expressing microglia in the retina allows quantification of microglia density in vivo, and yields similar results to microglia nuclear counts on retinal flat mounts. In addition, we showed that widefield AF imaging in these mice is reproducible and can be used to detect longitudinal changes in microglia density.

Imaging with the 102° widefield lens captured roughly three times the area covered with the 55° lens. In mouse

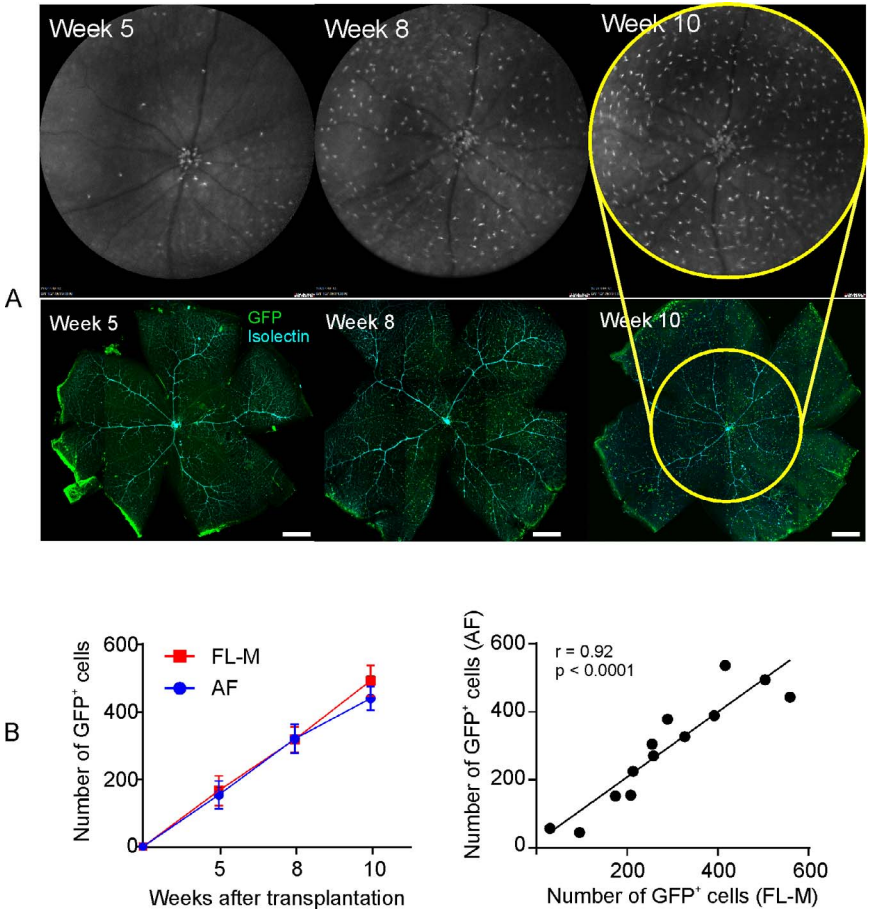

Figure 3. Longitudinal quantification of retinal microglia on AF and flat mount images after lethal irradiation and *Cx3cr1*$^{gfp/gfp}$ bone marrow reconstitution (**A**) Representative AF images (*upper panel*) and flat mounts stained with gfp and Isolectin GS-IB4 (*bottom panel*) at the indicated time points after bone marrow transplantation. Data from corresponding regions of interest were quantified (*yellow circles*, *right panel*). (**B**) Quantification of gfp-positive cells and correlation between retinal flat mounts and AF ($n \geq 4$ per time point). No statistically significant difference was observed between retinal flat mounts and AF cell numbers at any time point ($P > 0.05$, paired *t*-test).

models with retinal changes not only at the posterior pole, such as oxygen-induced retinopathy[17] or experimental retinal vein occlusion,[18] the peripheral microglia is of great interest, and widefield imaging seems particularly advantageous. We have previously reported on the dynamics of activated microglia and macrophages in transgenic mice in the latter model.[19] Significant changes were found in the peripheral retina, which would have escaped our attention using conventional optics. Hence, widefield imaging tools are crucial for the assessment of experimental outcomes in such models. However, despite using the 102° widefield lens, approximately half of the retina is still not represented in a single field of view. However, by rotating the lens to different angles or by repositioning the mouse on the platform, much of the peripheral retina can also be imaged.

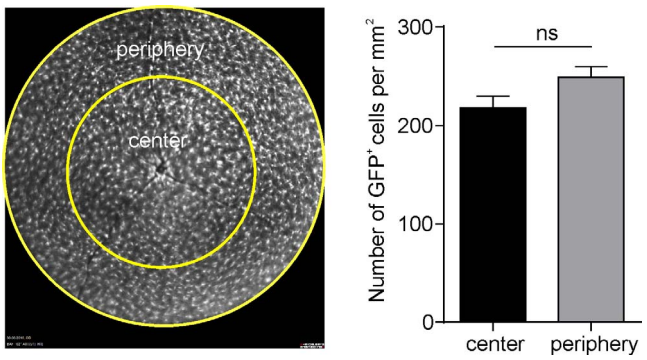

Figure 4. Quantification of gfp-positive cell density in the central (area imaged with the 55°) and peripheral retina. No statistically significant difference was observed on gfp-positive cells density ($n = 10$, $P > 0.05$, paired *t*-test).

In the DBA/2J mouse model of chronic glaucoma, it has been shown that even morphologic changes accompanying activation of microglia can be quantified using the 55° lens in vivo.[20] Although we did not investigate morphologic change occurring with microglial activation in this study, we established that the resolution of individual cells with the 102° widefield lens appeared to be comparable to the performance of the 55° optics, and that quantification of microglia density in vivo correlated equally well with data from retinal flat mounts for both lenses. In vivo imaging of microglia that substitutes flat mount preparations and confocal imaging results in important time savings, makes laboratory resources available for other tasks, and greatly reduces the usage of laboratory mice.

Finally, widefield imaging in combination with bone marrow grafting from *Cx3cr1*$^{gfp/gfp}$ mice was used to monitor reconstitution of the microglia population in lethally irradiated wildtype Balb/c mice. The time course of reconstitution on flat mounts using confocal microscopy closely resembled that seen in AF imaging in vivo. Previous reports have shown that microglia replenishment occurs as early as 4 weeks after

transplantation,[21] but complete replacement may take up to 6 months.[4] Anyway, recent investigations in the brain have shown that the microglia turnover seems faster than previously thought,[22] and regional differences exist.[23] Recent studies suggest that under normal conditions, the microglia population in the central nervous system is maintained by resident cells rather than invading bone-marrow-derived precursors.[24,25] Widefield AF imaging using models with fluorescent labelled microglia precursors might be useful in investigating these processes in the retina, and could facilitate future studies about microglia homeostasis, but also investigations on pharmacologic microglia modulation and depletion.

In summary, in vivo imaging seems a useful tool to quantify microglia in the retina, and cell density measurements correlate well with ex vivo microglia counts on flat mounts. Widefield imaging considerably increases the captured area of the retina, is easily feasible without hardware modifications, and results in significant savings of laboratory resources.

Acknowledgments

Supported by a grant of the Swiss National Science Foundation (SNSF) (#320030_156019). A. Ebneter is supported by a CTU Research-Grant (84800858) and the Dr. Streuli-Fonds, Bern, Switzerland. The sponsor or funding organization had no role in the design or conduct of this research.

Disclosure: **D. Kokona**, Bayer (F); **N. Schneider**, None; **H. Giannakaki-Zimmermann**, None; **J. Jovanovic**, None; **A. Ebneter**, Allergan (C, R), Bayer (R), Novartis (F, R), Plexxikon, Inc. (F); **M. Zinkernagel**, Bayer (C, F), Heidelberg Engineering (S), Novartis, (C, I), Plexxikon, Inc. (F)

References

1. Zinkernagel MS, Chinnery HR, Ong ML, et al. Interferon gamma-dependent migration of microglial cells in the retina after systemic cytomegalovirus infection. *Am J Pathol*. 2013; 182:875–885.
2. Ransohoff RM, Perry VH. Microglial physiology: unique stimuli, specialized responses. *Annu Rev Immunol*. 2009; 27:119–145.
3. Eandi CM, Charles Messance H, Augustin S, et al. Subretinal mononuclear phagocytes induce cone segment loss via IL-1beta. *eLife*. 2016;5.
4. Xu H, Chen M, Mayer EJ, Forrester JV, Dick AD. Turnover of resident retinal microglia in the normal adult mouse. *Glia*. 2007;55:1189–1198.
5. Wang X, Zhao L, Zhang J, et al. Requirement for microglia for the maintenance of synaptic function and integrity in the mature retina. *J Neurosci*. 2016;36:2827–2842.
6. Thanos S. Sick photoreceptors attract activated microglia from the ganglion cell layer: a model to study the inflammatory cascades in rats with inherited retinal dystrophy. *Brain Res*. 1992;588:21–28.
7. Zhang C, Shen JK, Lam TT, et al. Activation of microglia and chemokines in light-induced retinal degeneration. *Mol Vis*. 2005;11:887–895.
8. Joly S, Francke M, Ulbricht E, et al. Cooperative phagocytes: resident microglia and bone marrow immigrants remove dead photoreceptors in retinal lesions. *Am J Pathol*. 2009;174: 2310–2323.
9. Ebneter A, Casson RJ, Wood JP, Chidlow G. Microglial activation in the visual pathway in experimental glaucoma: spatiotemporal characterization and correlation with axonal injury. *Invest Ophthalmol Vis Sci*. 2010;51:6448–6460.
10. Zeiss CJ, Johnson EA. Proliferation of microglia, but not photoreceptors, in the outer nuclear layer of the rd-1 mouse. *Invest Ophthalmol Vis Sci*. 2004;45:971–976.
11. Hughes EH, Schlichtenbrede FC, Murphy CC, et al. Generation of activated sialoadhesin-positive microglia during retinal degeneration. *Invest Ophthalmol Vis Sci*. 2003;44:2229–2234.
12. Ajami B, Bennett JL, Krieger C, Tetzlaff W, Rossi FM. Local self-renewal can sustain CNS microglia maintenance and function throughout adult life. *Nat Neurosci*. 2007;10:1538–1543.
13. Zhang P, Zam A, Jian Y, et al. In vivo wide-field multispectral scanning laser ophthalmoscopy-optical coherence tomography mouse retinal imager: longitudinal imaging of ganglion cells, microglia, and Müller glia, and mapping of the mouse retinal and choroidal vasculature. *J Biomed Opt*. 2015;20: 126005.
14. Jung S, Aliberti J, Graemmel P, et al. Analysis of fractalkine receptor CX(3)CR1 function by targeted deletion and green fluorescent protein reporter gene insertion. *Mol Cell Biol*. 2000;20:4106–4114.
15. Kaschke M, Donnerhacke KH, Rill MS. *Optical Devices in Ophthalmology and Optometry: Technology, Design Principles and Clinical Applications*. 1st ed. Weinheim, Germany: Wiley; 2014.
16. Schneider CA, Rasband WS, Eliceiri KW. NIH Image to ImageJ: 25 years of image analysis. *Nat Methods*. 2012;9:671–675.
17. Fischer F, Martin G, Agostini HT. Activation of retinal microglia rather than microglial cell density correlates with retinal neovascularization in the mouse model of oxygen-induced retinopathy. *J Neuroinflammation*. 2011;8:120.
18. Ebneter A, Agca C, Dysli C, Zinkernagel MS. Investigation of retinal morphology alterations using spectral domain optical coherence tomography in a mouse model of retinal branch and central retinal vein occlusion. *PLoS One*. 2015;10: e0119046.
19. Ebneter A, Kokona D, Schneider N, Zinkernagel MS. Microglia activation and recruitment of circulating macrophages during ischemic experimental branch retinal vein occlusion. *Invest Ophthalmol Vis Sci*. 2017;58:944–953.
20. Bosco A, Romero CO, Ambati BK, Vetter ML. In vivo dynamics of retinal microglial activation during neurodegeneration: confocal ophthalmoscopic imaging and cell morphometry in mouse glaucoma. *J Vis Exp*. 2015;99:e52731.
21. Kezic J, McMenamin PG. Differential turnover rates of monocyte-derived cells in varied ocular tissue microenvironments. *J Leukoc Biol*. 2008;84:721–729.
22. Askew K, Li K, Olmos-Alonso A, et al. Coupled proliferation and apoptosis maintain the rapid turnover of microglia in the adult brain. *Cell Rep*. 2017;18:391–405.
23. Mittelbronn M, Dietz K, Schluesener HJ, Meyermann R. Local distribution of microglia in the normal adult human central nervous system differs by up to one order of magnitude. *Acta Neuropathol*. 2001;101:249–255.
24. Elmore MR, Najafi AR, Koike MA, et al. Colony-stimulating factor 1 receptor signaling is necessary for microglia viability, unmasking a microglia progenitor cell in the adult brain. *Neuron*. 2014;82:380–397.
25. Bruttger J, Karram K, Wortge S, et al. Genetic cell ablation reveals clusters of local self-renewing microglia in the mammalian central nervous system. *Immunity*. 2015;43:92–106.